

# Cavity-modified unimolecular dissociation reactions *via* intramolecular vibrational energy redistribution

Derek S. Wang,<sup>1,\*</sup> Tomáš Neuman,<sup>2</sup> Susanne F. Yelin,<sup>3,†</sup> and Johannes Flick<sup>4,‡</sup>

<sup>1</sup>*Harvard John A. Paulson School of Engineering and Applied Sciences,  
Harvard University, Cambridge, MA 02138, USA*

<sup>2</sup>*IPCMS de Strasbourg, UMR 7504 (CNRS – Université de Strasbourg), 67034 Strasbourg, France*

<sup>3</sup>*Department of Physics, Harvard University, Cambridge, MA 02138, USA*

<sup>4</sup>*Center for Computational Quantum Physics, Flatiron Institute, New York, NY 10010, USA*

(Dated: March 15, 2022)

While the emerging field of vibrational polariton chemistry has the potential to overcome traditional limitations of synthetic chemistry, the underlying mechanism is not yet well understood. Here, we explore how the dynamics of unimolecular dissociation reactions that are rate-limited by intramolecular vibrational energy redistribution processes can be modified inside an infrared cavity. We study a classical model of a bent triatomic molecule, where the two outer atoms are bound by anharmonic Morse potentials to the center atom. We show how energy-dependent anharmonic resonances emerge and that resonantly coupling the optical cavity to particular dynamical resonance traps can either significantly slow down or increase the intramolecular vibrational energy redistribution processes depending on the strength of vibrational momentum-momentum mode coupling, leading to altered unimolecular dissociation reaction rates. These results demonstrate that chemical reactivity can be modified inside a cavity and lay the foundation for further theoretical work toward understanding the intriguing experimental results of vibrational polariton chemistry.

## I. INTRODUCTION

Mode-selective chemistry—exciting just a single bond in a molecule to control its chemical properties—is a long sought-after goal [1–6] that would allow selective control over chemical reactivity and energy transfer for applications in, *e.g.*, the production of industrial chemicals and pharmaceuticals, photosynthesis, or conversion of renewable energy sources. Realization of this goal has generally been hampered, however, by intramolecular and intermolecular vibrational energy redistribution that limits the efficiency of a mode-selective excitation beyond cryogenic temperatures [7]. Interest in this field was revitalized with the emergence of the field of vibrational polariton chemistry [8–18]. Changes of reaction rates of molecules inserted into infrared cavities have been observed experimentally, demonstrating the influence of the resonant coupling of molecular infrared-active vibrations with the electromagnetic vacuum of the cavity on the underlying reaction dynamics. Despite intense efforts to understand why the reaction rate changes [19–26], the microscopic mechanisms underlying the experimental observations are still under debate.

Recent studies have hinted at the role of intramolecular vibrational energy redistribution (IVR) in cavity-modified chemical reactions studied *via* first-principles methods [24, 27] or molecular dynamics simulations [28–31]. The role of vibrational strong coupling on the chemical reactivity of 1-phenyl-2-trimethylsilylacetylene

(PTA) using quantum electrodynamic density functional theory [32, 33] was able to replicate some of the effects observed experimentally by Thomas *et al.* [34]. However, due to the computational complexity, these methods still face certain limitations, such as in the number of simulated trajectories or possible reaction pathways.

Therefore, in this work, we theoretically study cavity-modified unimolecular dissociation reactions with a classical model of a molecule. We show that by coupling the infrared-active modes of the molecule to the cavity vacuum it is possible to both slow down and speed up the rate of bond dissociation in individual molecules.

## II. MODEL FOR UNIMOLECULAR DISSOCIATION

In this section, we first develop an understanding of IVR-mediated dissociation dynamics of the bare molecule, meaning that the molecule is located outside an optical cavity. We use a classical triatomic model with three degrees of freedom and anharmonic potentials. This model was previously used by Karmakar *et al.* to understand the onset of chaos in IVR processes [35] and is itself based on the approach pioneered by D. L. Bunker and others who studied the ozone molecule in a series of computational studies on unimolecular dissociation reactions [36–38]. Importantly, this model is minimal while still demonstrating chaotic dynamics through an interconnected Arnold web [39, 40], or network of nonlinear resonances, and therefore serves as a fundamental starting point for IVR studies of larger molecules. The Hamiltonian for the model system can be written in terms of

---

\* derekwang@g.harvard.edu

† syelin@physics.harvard.edu

‡ jflick@flatironinstitute.org

the local vibrational modes as

$$H_{\text{mol}} = \sum_{i=1}^3 \left[ \frac{1}{2} G_{ii}^{(0)} p_i^2 + V_i(q_i) \right] + \epsilon \sum_{i<j=2}^3 G_{ij}^{(0)} p_i p_j, \quad (1)$$

where  $i \in \{1, 2, 3\}$  correspond to the local stretching mode between the left atom and the center atom, the local stretching mode between the center atom and the right atom, and the local bending mode, respectively. The position coordinates  $q_i$  for  $i = 1$  and  $2$  are in units of distance, while  $q_3$  is in units of angle, and  $p_i$  are their respective conjugated momentum coordinates. A schematic of the model system and the coordinates is depicted in Fig. 1(a). The coupling element  $G_{ij}^{(0)}$  between momenta  $p_i$  and  $p_j$  is due to the transformation from normal mode coordinates, where we consider collective motions of nuclei, to local mode coordinates, where we focus on the movement of specific parts of the molecule [41]. This momentum-momentum interaction is scaled by  $\epsilon$ , roughly corresponding to *e.g.* varying the mass of the center atom relative to the other two atoms [36], to explore the effect of varying vibrational mode-mode momentum couplings. For non-zero  $\epsilon$ , the local vibrational modes  $q_1, q_2$  and  $q_3$  do not correspond to normal (or eigen-) modes of the system. In addition, note that the coordinate-dependent  $G_{ij}$  in the original model of Bunker [36] are replaced with their equilibrium values  $G_{ij}^{(0)}$ , and that this model is fixed in the  $x$ - $y$  plane with dipole activity only in the  $x$ - and  $y$ -directions, although the rovibronic couplings have also been shown to impact IVR in certain circumstances [42]. For the two stretching modes  $i = 1, 2$ , the vibrational potential is approximated by a Morse potential:  $V_i(q_i) = D_i \{1 - \exp(-\alpha_i [q_i - q_i^0])\}^2$ , where  $D_i$  is the dissociation energy,  $\alpha_i$  controls the anharmonicity of the potential well and the number of bound vibrational states in a quantum picture,  $q_i^0$  is the equilibrium atom-atom distance, and  $\omega_i$  is the frequency of the potential well under the low-displacement or harmonic approximation. For the bending mode, the vibrational potential is assumed to be harmonic:  $V_3(q_3) = \omega_3^2 (q_3 - q_3^0)^2 / (2G_{33}^{(0)})$ , valid for low displacements.

From  $H_{\text{mol}}$  in Eq. 1, the equations of motion can be derived and stably propagated given a set of initial coordinates up to several tens of picoseconds using the 8th order Runge-Kutta method [43]. When the molecule is initialized with energy exceeding the dissociation energy  $D_i$ , it is possible for the molecule to dissociate. We define successful dissociation when either  $q_1$  or  $q_2$  exceeds a bond length of 5 Bohr from the equilibrium value  $q_1^0$  or  $q_2^0$ . We show an example trajectory that leads to dissociation in Fig. 1(b), where we plot the deviation of the molecular coordinates  $q_i$  from their equilibrium positions  $q_i^0$ . Here, the initial energy is 34 kcal/mol  $> D_1 = D_2 = 24$  kcal/mol,  $(\omega_1, \omega_2, \omega_3) = (1112, 1040, 632)$  cm $^{-1}$ ,  $\alpha_1 = 2.212$  Bohr $^{-1}$ ,  $\alpha_2 = 2.069$  Bohr $^{-1}$ , and equilibrium values  $q_i^0$  and  $G_{ij}^{(0)}$  are as defined in Table I in Appendix A and in Ref. 35. The trajectory exhibits chaotic

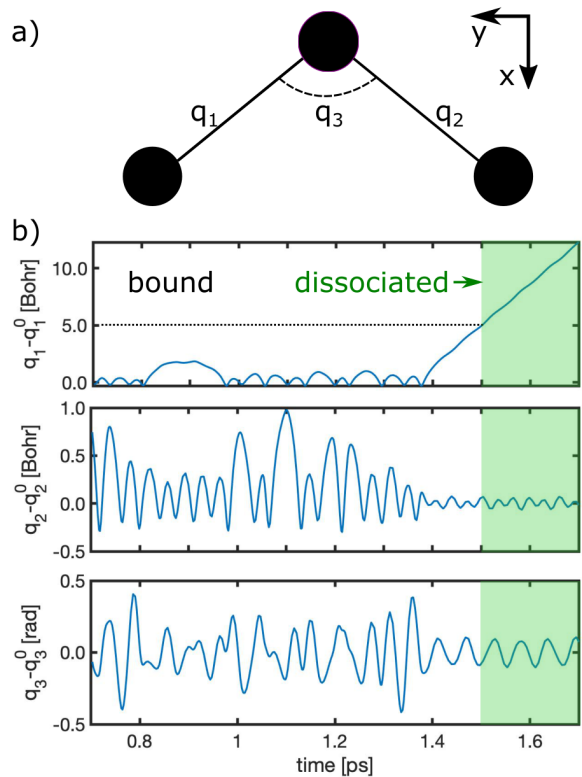


**FIG. 1.** (a) Schematic of the model triatomic model in a cavity with local mode coordinates  $q_1$  (stretch length between left and center atoms),  $q_2$  (stretch length between center and right atoms), and  $q_3$  (bending angle between bonds of left-center atoms and center-right atoms). (b) Example of a trajectory initialized with energy of 34 kcal/mol, greater than dissociation energy  $D_i$ . Local mode displacements  $q_i - q_i^0$  are in atomic units. The molecule dissociates at  $\sim 1.5$  ps, marked by the green region, when  $q_1 - q_1^0$  exceeds dissociation length  $r_{\text{dis}} = 5$  Bohr.

oscillation of the internal coordinates of the molecule resulting finally in the divergence of the bond length  $q_1$ , and therefore dissociation of the molecule.

To understand the IVR dynamics of the bare molecule, we calculate the frequency spectra  $q_i(\omega_k) = \sum_{j=0}^{N-1} [q_i(t_j) - q_i^0] \exp(-2\pi i k j / N)$  for  $j, k \in \{0, \dots, N-1\}$  where  $N$  is the number of discrete points. This expression corresponds to the one-sided discrete Fourier transform of the trajectories  $q_i(t) - q_i^0$  propagating under  $H_{\text{mol}}$ . We also plot the  $x$ - and  $y$ -polarized dipole moments  $\boldsymbol{\mu}(t) - \boldsymbol{\mu}_0$  that correspond to an infrared spectrum by Fourier transforming the time-dependent dipole moment. Choosing the  $x$ -axis to be in-plane and through the center atom along  $q_3^0/2$ , as in Fig. 1(a), we parametrize the permanent dipole moment as  $\boldsymbol{\mu} = A[\cos(q_3/2)(q_1 + q_2)\hat{x} + \sin(q_3/2)(q_1 - q_2)\hat{y}]$ , where  $\hat{x}$  and  $\hat{y}$  are the corresponding unit vectors, and the constant  $A$  is chosen such that the equilibrium permanent dipole moment  $\boldsymbol{\mu}_0$  in the  $x$ -direction is 1 e-Bohr, on the order of the permanent dipole moment for bent triatomic molecules, such as ozone [44, 45]. In Fig. 5 in the Appendix, we describe

signatures of the emergence of both vibrational mode-mode momentum coupling with non-zero  $\epsilon$  and anharmonic resonances beyond the harmonic approximation with increasing molecule energy.

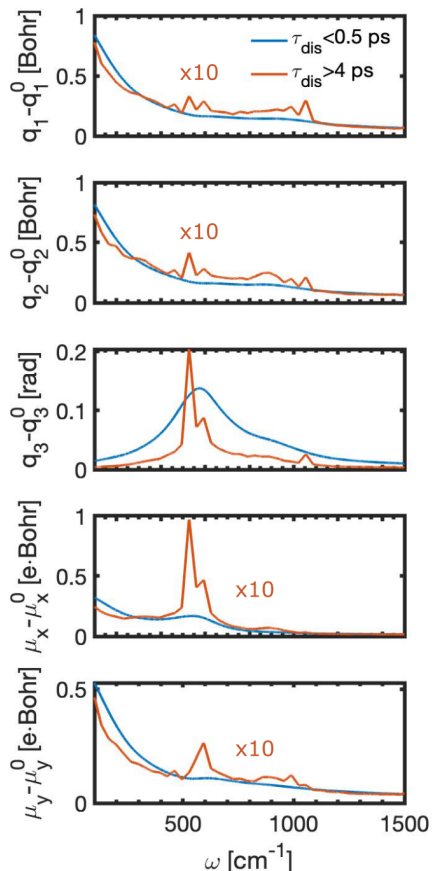


**FIG. 2.** Frequency spectra of displacements  $q_i - q_i^0$  and permanent dipole moment  $\mu - \mu_0$  outside the cavity, in atomic units, for  $\epsilon = 1$  and total energy  $E = 34$  kcal/mol  $> D_i$  corresponding to coupled anharmonic oscillators. We average the Fourier transform of 219,126 trajectories pre-dissociation with dissociation lifetimes  $< 0.5$  ps (blue) and 315 trajectories with dissociation lifetimes  $> 4$  ps (orange), normalizing spectrum intensities by the number of trajectories. Note that the intensities for  $\tau_{\text{dis}} > 4$  ps are multiplied by 10 for  $q_1 - q_1^0$ ,  $q_2 - q_2^0$ ,  $\mu_x - \mu_x^0$ , and  $\mu_y - \mu_y^0$  to better highlight the spectral features.

In Fig. 2, we plot the frequency spectra for molecules initialized with energy 34 kcal/mol  $> D_i = 24$  kcal/mol, sufficient to dissociate the bond. To statistically characterize the influence of model parameters on the dissociation lifetimes and the chaotic dynamics of the IVR processes [35–37], we propagate the trajectories for  $\sim 10^4 - 10^5$  initial states of identical energies [35] and bin them by their dissociation lifetimes.

We show two bins of trajectories in Fig. 2, those with lifetimes  $< 0.5$  ps (blue) and those with lifetimes  $> 4$  ps (orange). The frequency spectra of the local stretching modes  $q_1$  and  $q_2$  are nearly uniformly distributed but in-

creasing toward lower frequencies due to large displacements from equilibrium inside the Morse potentials and therefore smaller frequency spacing between vibrational states. Notably, for the short-lived trajectories we observe smooth spectral dependence which hints towards the statistical decay dynamics in which the many anharmonic resonances of the local vibrational modes are explored quickly and at random. In contrast, the Fourier spectra of the long-lived trajectories feature a number of peaks (at  $\sim 500$   $\text{cm}^{-1}$  and  $\sim 1000$   $\text{cm}^{-1}$ ) that represent resonant “traps” preferentially visited during the system time evolution. The frequency spectrum of the local bending mode  $q_3$  for the short-lived trajectories is also distributed across the entire frequency space, verifying the statistical nature of the decay, although there is a broad peak in the 500  $\text{cm}^{-1}$  to 700  $\text{cm}^{-1}$  range corresponding roughly to the harmonic resonance of the bending mode. In contrast, the spectra of  $q_3$  obtained from the long-lived trajectories are dominated by sharp peaks at  $\sim 510$   $\text{cm}^{-1}$  and  $\sim 580$   $\text{cm}^{-1}$  reflecting the non-statistical nature of the dynamics. Finally, the spectral features appearing in the Fourier transforms of the dipole moments  $\mu_x$  and  $\mu_y$  closely reflect the behavior of the bending ( $q_3$ ), and stretching ( $q_1$  and  $q_2$ ) coordinates, respectively.

The appearance of sharp resonances for long-lived trajectories strongly suggests that long survival lifetimes are a result of dynamical trapping inside these resonances. This interpretation has been proposed by Karmakar *et al.*, suggesting that molecules initialized near these anharmonic resonances live longer, and, conversely, trajectories with longer lifetimes spend proportionally more time inside these resonances than those with shorter lifetimes. The existence of such resonant “traps” strongly depends on the intrinsic properties of the molecule, including the relative tuning of vibrational frequencies. Here we suggest to modify these properties by placing the molecule into an infrared electromagnetic cavity whose field interacts strongly with the infrared-active molecular vibrations. In the next section we therefore extend the model of IVR to include the effect of light-matter coupling on the anharmonic vibrational dynamics and demonstrate the consequences of the model.

### III. SLOWER IVR DYNAMICS IN A RESONANT CAVITY

To incorporate the effect of light-matter coupling between the electric field of an infrared cavity and the vibrations of the molecular model, we add the classical field Hamiltonian  $H_F$ , which becomes the Pauli-Fierz Hamiltonian in its quantized form [32]:

$$H_F = \sum_k \left[ \frac{1}{2} p_k^2 + \frac{1}{2} \omega_k^2 \left( q_k - \frac{\lambda_k}{\omega_k} \boldsymbol{\mu} \cdot \boldsymbol{\xi} \right)^2 \right], \quad (2)$$

where  $\omega_k$ ,  $q_k$ ,  $p_k$ ,  $\lambda_k$  are the frequency, displacement, momentum, and strength of the cavity mode  $k$ ,  $\boldsymbol{\mu}$  is the permanent dipole moment of the molecule, and  $\boldsymbol{\xi}$  is the unit

vector of polarization of the electric field. We note that a similar approach has been taken in classical molecular dynamics studies of polaritonic chemistry [28, 29].

We first study the scenario where the molecular vibrations of the model with  $\epsilon = 1$  and energy of 34 kcal/mol are coupled to a single cavity mode with frequency  $\omega_c$  and with cavity strength  $\lambda_c$  oriented along the direction  $\theta$  from the  $x$ -axis. Noting that the dipole moment along the  $x$ -direction is strongest at  $512 \text{ cm}^{-1}$ , as we see in the plot for  $\mu_x - \mu_x^0$  in Fig. 2, we maximize the strength of light-matter coupling for a given  $\lambda_c$  by polarizing the cavity field along the  $x$ -direction and setting  $\omega_c = 512 \text{ cm}^{-1}$ . We vary the cavity strength  $\lambda_c$  and plot the (natural logarithm of) the survival probability  $S(t)$ , or the proportion of initial states that have not dissociated as a function of time in Fig. 3(a), as well as the time required for 95% of the molecules initialized with 34 kcal/mol to dissociate in Fig. 3(b). Both figures clearly show that the decay rate decreases as  $\lambda_c$  is increased from 0 to 0.012 a.u. For reference,  $\lambda_c = 0.01$  a.u. corresponds to a single-mode Rabi splitting of  $\sim 10 \text{ cm}^{-1}$  (see Appendix C for further details).

We also note that the form of the decay curve changes substantially. For  $\lambda_c = 0$  corresponding to complete decoupling between the molecule and the cavity,  $\ln(S(t))$  is best described through mono-exponential decay  $\sim e^{-t/\tau_1}$  with lifetime  $\tau_1$ , closely matching the results of Fig. 1a in Ref. 35. As Karmakar *et al.* note, under these conditions, distribution of vibrational energy occurs mostly statistically, meaning that the space of nonlinear frequency resonances between vibrational modes is widely explored with little trapping in any particular nonlinear resonance. As  $\lambda_c$  increases to 0.01 atomic units, however,  $S(t)$  veers away from mono-exponential decay and is instead better described with bi-exponential decay  $\sim f_1 e^{-t/\tau_1} + f_2 e^{-t/\tau_2}$ , where  $f_1$  and  $f_2$  weight the contributions of the faster timescale  $\tau_1$  and slower one  $\tau_2$ . The cavity may be enhancing IVR-limited decay by serving as a sink for vibrational energy, lowering the probability that one of the stretch bonds acquires enough energy to break.

We further explore the cavity-coupled Bunker model by again coupling the molecular vibrations to a single cavity mode, but this time with constant cavity strength  $\lambda_c = 0.01$  a.u. and varying cavity frequency  $\omega_c$  from  $100 \text{ cm}^{-1}$  to  $1100 \text{ cm}^{-1}$ . From Fig. 3(c), we see that for much of this frequency range, the  $S(t)$  curves look similar to the case of  $\lambda_c = 0$  a.u. in Fig. 3(a), where the decay is best fitted by a mono-exponential curve indicating statistical decay. In the frequency range from  $500 \text{ cm}^{-1}$  to  $600 \text{ cm}^{-1}$ , however, the reaction dynamics are strongly changed. To study them with a finer frequency resolution in this range, we plot the time required for 95% dissociation in Fig. 3(d), where we observe peaks at  $\sim 510 \text{ cm}^{-1}$  and  $\sim 580 \text{ cm}^{-1}$ , the same frequencies of the peaks  $\mu_x - \mu_x^0$  in Fig. 5 and therefore serving as direct evidence of a resonant effect.

We also explore the effect of coupling to a different

resonance trap. The  $y$ -polarized infrared spectrum and, thus, light-matter coupling strength are also high near  $\sim 900 \text{ cm}^{-1}$ , away from the resonance trap at  $512 \text{ cm}^{-1}$  we explore in Fig. 3(c)-(d). We set a constant cavity strength  $\lambda_c = 0.05$  a.u. along the  $y$ -direction, which is scaled higher than  $\lambda_c = 0.01$  a.u. for the study of the  $x$ -polarized cavity because the  $y$ -polarized infrared spectrum in Fig. 2(f) is smaller than the  $x$ -polarized counterpart. We then vary the cavity frequency  $\omega_c$  from  $100 \text{ cm}^{-1}$  to  $1100 \text{ cm}^{-1}$ . Here, we observe a broader resonant effect at a different frequency of  $\sim 900 \text{ cm}^{-1}$ , corresponding to the broader peak in the  $y$ -polarized infrared spectrum, as opposed to the sharper double peak  $\sim 510 \text{ cm}^{-1}$  and  $580 \text{ cm}^{-1}$  in Fig. 3(c)-(d) where the cavity field is oriented along the  $x$ -direction.

#### IV. ACCELERATING CHEMICAL REACTIONS

Thus far, we have observed slower IVR reaction rates, but as we demonstrate now, accelerated rates can be achieved as well. To that end, we calculate the decay time of the initial reactants by varying  $\epsilon \in \{1.0, 0.3, 0.1, 0.01\}$  with fixed cavity strength  $\lambda_c$  in Fig. 4. The survival probability thresholds  $S_{\text{th}} \in \{0.05, 0.2, 0.6, 0.7\}$  differ for each  $\epsilon$  because as  $\epsilon$  decreases, the timescale of decay increases, resulting in increased computational cost. Also, we note that lower  $\epsilon$  roughly corresponds to *e.g.* higher mass of the center atom relative to the other two atoms [36]. For  $\epsilon = 1.0, 0.3$ , and  $0.1$ , the time  $t_{\text{th}}$  to reach  $S_{\text{th}}$  inside the cavity is larger, or the reaction rate decreases, whereas for  $\epsilon = 0.01$ , the time to  $S(t) = 0.75$  can also decrease at a particular resonance frequency. Hence, the reaction rate can be faster. This effective increase of the reaction rate can be interpreted as follows: for large  $\epsilon$ , the dynamics of energy distribution are dominated by vibrational mode-mode momentum coupling, whereas for small  $\epsilon \ll 1$ , the dynamics are dominated by coupling to the cavity, which then can assist in transferring energy between vibrational modes.

The case of relatively small  $\epsilon$  can be loosely analogized to the case of *intermolecular* vibrational energy redistribution, since the energies of intermolecular interactions are one to three orders of magnitude lower than intramolecular ones. Alternatively, the weak mode-mode momentum couplings could represent coupling to low-frequency intramolecular vibrational modes known to serve as baths for vibrational energy [7]. Regardless of the interpretation, the results in Fig. 4 demonstrate that the cavity mode can effectively augment the coupling between vibrational modes and accelerate the reaction rate. These results may be relevant to the studies showing enhanced reaction rates when tuning the cavity into resonance with a vibrational mode of solvent molecules [46, 47] that are vibrationally weakly coupled to reactant molecules outside the cavity.

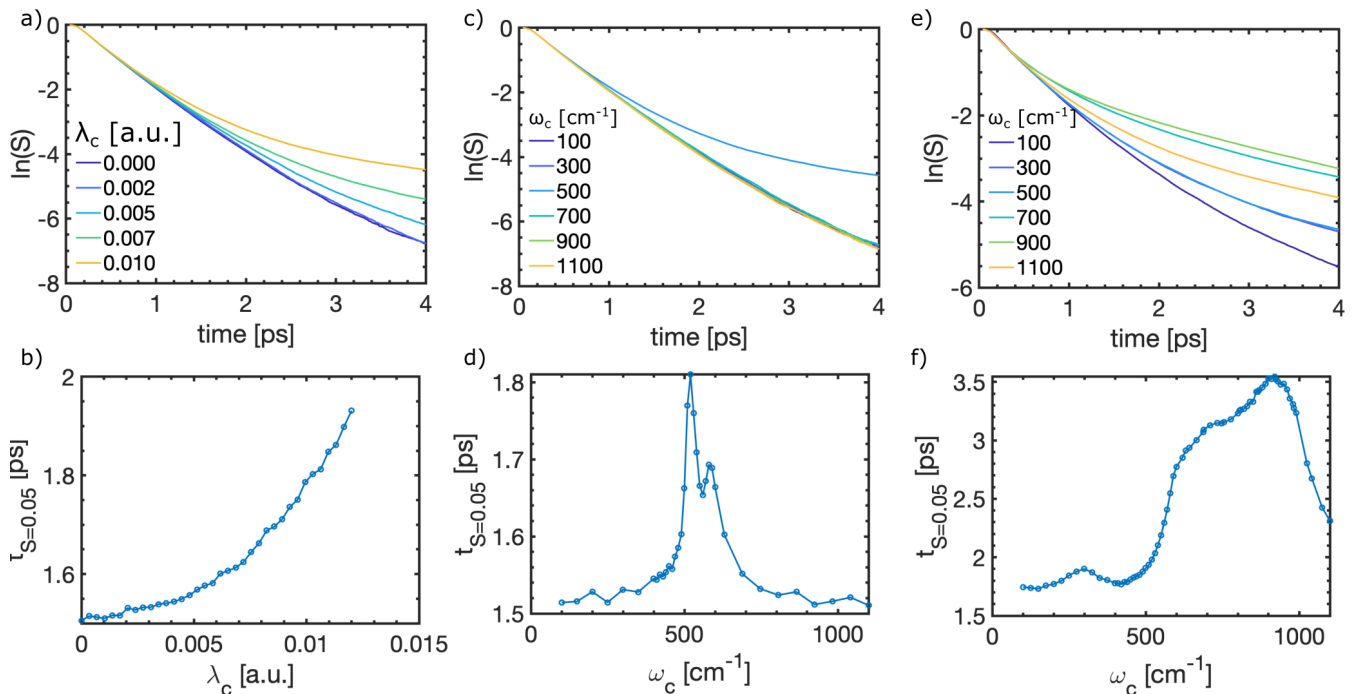


**FIG. 3.** Cavity-modified unimolecular dissociation rate with survival probability as a function of time (top) and time required for 95% of molecules with initial energy of 34 kcal/mol (bottom). In **(a)-(b)**, we vary the cavity strength  $\lambda_c$  for  $\omega_c = 512 \text{ cm}^{-1}$  and  $x$ -polarized cavity field, resulting in the dissociation rate slowing down with increasing cavity strength. At higher cavity strength  $\lambda_c$ , the cavity and molecular vibrational modes are more strongly coupled together. In **(c)-(d)**, the cavity frequency  $\omega_c$  is varied for  $\lambda_c = 0.01$  and  $x$ -polarized cavity field; the dissociation rate slows down at  $\omega \sim 510$  and  $\sim 580 \text{ cm}^{-1}$ , the same frequencies of the peaks in  $\mu_x - \mu_x^0$  in Fig. 2. In **(e)-(f)**, we vary cavity frequency  $\omega_c$  for  $\lambda_c = 0.05$  and  $y$ -polarized cavity field, resulting in a broadly resonant rate slow-down at centered  $\sim 900 \text{ cm}^{-1}$ , corresponding to peaks present in  $\mu_y - \mu_y^0$  but not  $\mu_x - \mu_x^0$  in Fig. 2.

## V. CONCLUSIONS AND OUTLOOK

In summary, we study a classical model of a triatomic molecule in an optical cavity based on a Bunker model, where the potential of the two local stretches are anharmonic Morse potentials and the local bending mode is harmonic. We extend this model by resonantly coupling the vibrational states with large optical dipole moments to a single electromagnetic mode of an infrared cavity. We demonstrate that this light-matter coupling can significantly slow down or speed up the rate of IVR-mediated unimolecular dissociation reactions. These results lay the foundation for further theoretical work toward understanding the intriguing experimental results of vibrational polariton chemistry.

The model can also be extended to more general situations. For instance, the ensembles of initial states used to calculate the dissociation dynamics can be selected through a variety of means. Here we study ensembles of trajectories picked from constant energy hypersurfaces [35]. Our approach can easily be generalized to differently chosen ensembles of initial states, however. For instance, to simulate conditions of vibrational excitation at room-temperature, energies and momenta can be selected from a Boltzmann distribution. Alternatively, to

simulate population *via* infrared laser pumping, only optically accessible initial states can be chosen.

Second, experimental demonstrations of vibrational polariton chemistry rely on the collective coupling of many molecules to the cavity mode to achieve the Rabi splittings observed in the infrared spectra on the order of  $10 \text{ cm}^{-1} - 100 \text{ cm}^{-1}$ . It is thus desirable to extend our model considering a single molecule to the collective case and explore the effects of disorder [25], or ensemble-enhanced coupling of the cavity mode to a single molecule [48, 49], among others. Moving forward, we expect molecular dynamics studies of many molecules inside an optical cavity that also include molecular translational and rotational degrees of freedom and intramolecular IVR interactions [28–31, 50, 51] with a particular focus on IVR dynamics to be fruitful.

Third, while for computational feasibility and ease of interpretation, we consider only a triatomic anharmonic model that serves as a minimal viable model for chaotic dynamics, molecules studied in experiments are considerably more complex. They can contain  $\sim 100$  vibrational degrees of freedom, and in cases when their dissociation energy becomes comparable to the quantum of vibrational energy, quantum effects can play an important role in the dissociation dynamics [34]. In such cases a quantum description, e.g. *via* first-principles method such

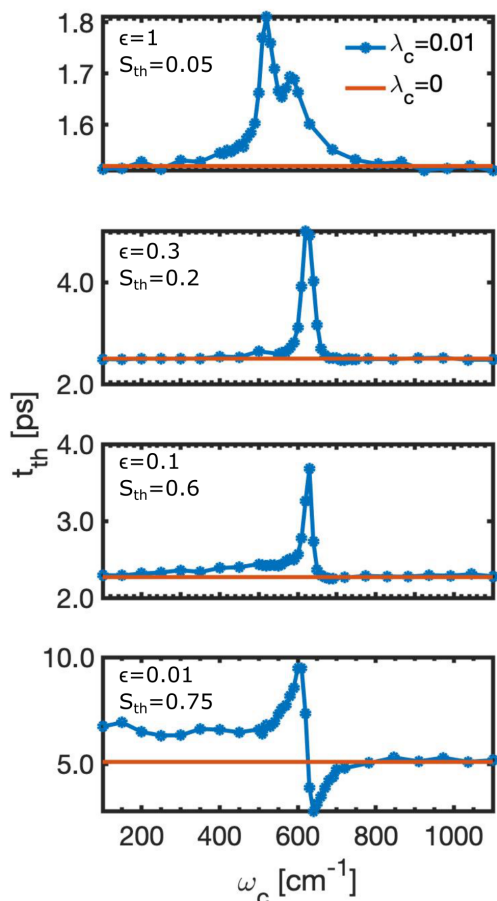


**FIG. 4.** Time  $t_{\text{th}}$  required for survival probability threshold  $S_{\text{th}}(t) = 0.05, 0.2, 0.6,$  and  $0.75$  as a function of cavity frequency for vibrational mode-mode momentum coupling  $\epsilon = 1, 0.3, 0.1,$  and  $0.01,$  respectively. The blue line corresponds to the molecule inside the cavity with varying frequency  $\omega_c$  and cavity strength  $\lambda_c = 0.01,$  and the red line corresponds to the molecule outside the cavity, or  $\lambda_c = 0.$  At larger  $\epsilon = 1, 0.3,$  and  $0.1,$  the unimolecular dissociation rate only decreases inside a resonant cavity relative to outside the cavity, while at small  $\epsilon = 0.01,$  the unimolecular dissociation rate can also be increased.

as quantum electrodynamical density functional theory [24, 32, 33, 52–54] is necessary. Future studies should therefore determine, for instance, whether the observed cavity-modified chemical reactivity in this study is robust to these factors.

#### ASSOCIATED CONTENT

Code to reproduce the calculations in this paper are available at <https://github.com/drekwang/cavityIVR>.

#### ACKNOWLEDGEMENTS

S.F.Y and J.F. contributed equally to this manuscript. D.S.W. acknowledges valuable discussions with Arkajit Mandal, Srihari Keshavamurthy, Sourav Karmakar, Joel Yuen-Zhou, Matthew Du, Jorge Campos-Gonzalez-Angulo, Eric J. Heller, and Vamsi V. Varanasi. D.S.W. is an NSF Graduate Research Fellow. S.F.Y. would like to acknowledge funding by DOE, AFOSR, and NSF. Calculations were performed using the computational facilities of the Flatiron Institute. The Flatiron Institute is a division of the Simons Foundation.

#### Appendix A: Model parameters

|                               |                       |                        |                               |
|-------------------------------|-----------------------|------------------------|-------------------------------|
| $q_1^0$                       | $q_2^0$               | $q_3^0$                |                               |
| 2.426                         | 2.426                 | 2.039                  |                               |
| $G_{11}^{(0)} = G_{22}^{(0)}$ | $G_{33}^{(0)}$        | $G_{12}^{(0)}$         | $G_{13}^{(0)} = G_{23}^{(0)}$ |
| $6.85 \times 10^{-5}$         | $2.88 \times 10^{-5}$ | $-1.54 \times 10^{-5}$ | $1.26 \times 10^{-5}$         |

**TABLE I.** Equilibrium values  $q_i^0$  and  $G_{ij}^{(0)}$  in atomic units adapted from Ref. 35.

#### Appendix B: IVR Dynamics

Here, we show the frequency spectra of the position coordinates and dipole moments to understand the emergence of vibrational mode-mode momentum coupling and anharmonic resonances. In particular, we study the Fourier form  $q_i(\omega)$ , or frequency spectra, of the trajectories  $q_i(t)$  propagating under  $H_{\text{mol}}$  with varying energies, in Fig. 5. We start by studying the simplest case, where no mode-mode momentum coupling, *i.e.*  $\epsilon = 0$  in Eq. 1, is present in Fig. 5(a). In addition, we choose an initial state with low energy  $10^{-6}$  kcal/mol compared to both the harmonic frequencies  $\omega_i$  of the Morse potentials and the dissociation energies  $D_i$  of the local stretching modes, such that the Hamiltonian effectively corresponds to three decoupled harmonic oscillators. We also select the initial state such that the energy contributions are roughly equally distributed among the three decoupled vibrational modes  $q_1, q_2,$  and  $q_3.$  As expected, there is only one visible peak in the spectrum of each mode at  $\omega_1, \omega_2,$  and  $\omega_3,$  respectively. Notably, the  $x$ -polarized infrared spectrum shows more pronounced peaks at the frequency of the local bending mode  $q_3,$  while the  $y$ -polarized infrared spectrum corresponds shows stronger peaks at the frequencies of the local stretching modes  $q_1$  and  $q_2.$

In Fig. 5(b)-(e), we turn on the vibrational mode-mode momentum coupling by setting  $\epsilon = 1.$  For the same initial state with energy  $10^{-6}$  kcal/mol in Fig. 5(b) as in Fig. 5(a), this Hamiltonian effectively describes three coupled harmonic oscillators, we find that due to the mode-mode momentum coupling, the local vibrational

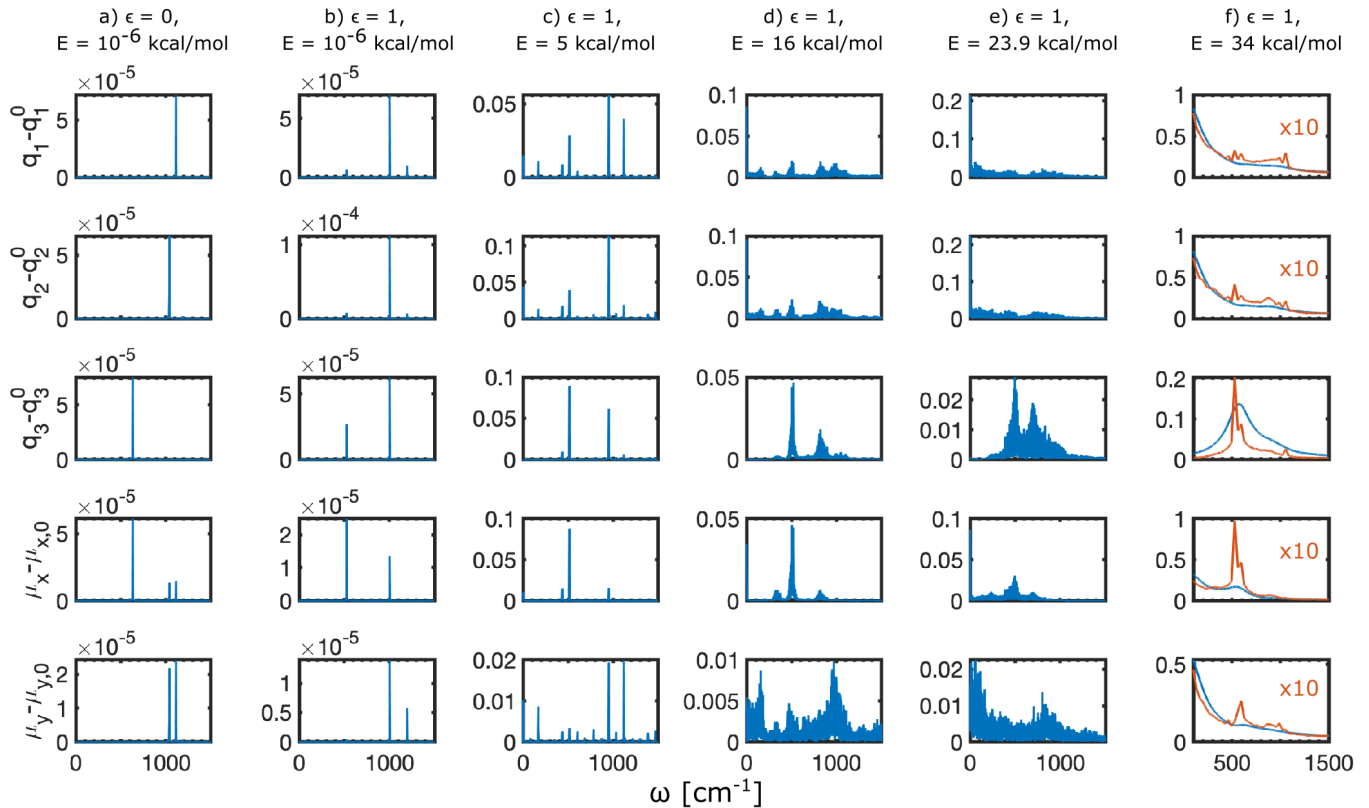


**FIG. 5.** Frequency spectra of displacements  $q_i - q_i^0$  and permanent dipole moment  $\mu - \mu_0$  outside the cavity, in atomic units, for **(a)**  $\epsilon = 0$  and initial state with total energy  $E = 10^{-6}$  kcal/mol  $\ll \omega_i$  corresponding to decoupled harmonic oscillators, **(b)**  $\epsilon = 1$  and total energy  $E = 10^{-6}$  kcal/mol  $\ll \omega_i$  corresponding to coupled harmonic oscillators, **(c)**  $\epsilon = 1$  and total energy  $E = 5$  kcal/mol  $< D_i = 24$  kcal/mol corresponding to coupled and bound anharmonic oscillators, **(d)**  $\epsilon = 1$  and total energy  $E = 16$  kcal/mol  $< D_i$  corresponding to coupled and highly excited anharmonic oscillators, **(e)**  $\epsilon = 1$  and total energy  $E = 23.9$  kcal/mol  $< D_i$  corresponding to coupled but nearly unbound anharmonic oscillators, **(f)**  $\epsilon = 1$  and total energy  $E = 34$  kcal/mol  $> D_i$  corresponding to coupled and unbound anharmonic oscillators. In (a)-(e), we Fourier transform single initial states propagating for 100 ps, whereas in (f), we average the Fourier transform of 219,126 trajectories pre-dissociation with dissociation lifetimes  $< 0.5$  ps (blue) and 315 trajectories with dissociation lifetimes  $> 4$  ps (orange), normalizing spectrum intensities by the number of trajectories. In (f), note that the  $x$ -axis starts at  $100$   $\text{cm}^{-1}$  vs.  $0$   $\text{cm}^{-1}$  in (a)-(e) and that the intensities for  $\tau_{\text{dis}} > 4$  ps are multiplied by 10 by  $q_1 - q_1^0$ ,  $q_2 - q_2^0$ ,  $\mu_x - \mu_x^0$ , and  $\mu_y - \mu_y^0$  to better highlight the spectral features.

modes are no longer the eigenmodes of the system—the actual eigenmodes are now “delocalized” over the three local modes and molecule, shifting the harmonic eigenfrequencies ( $\omega_1, \omega_2, \omega_3$  to  $(528, 1003, 1197)$   $\text{cm}^{-1}$  from  $(1112, 1040, 632)$   $\text{cm}^{-1}$  for  $\epsilon = 0$ . Note, however, that the two larger frequencies still comprise mostly stretching modes and smaller frequencies comprise mostly the bending mode. As the energy of the initial state is increased to 5 kcal/mol in Fig. 5(c), where  $q_1$  and  $q_2$  can explore more of the anharmonic Morse potential, we observe the emergence of further peaks corresponding to anharmonic resonances. In Fig. 5(d) with energy of 16 kcal/mol, the anharmonic resonances have broadened as the behavior is more chaotic and the intensities become more uniform across the frequency range. As the energy of the initial state is increased even further to 23.9 kcal/mol in Fig. 5(e), just below the dissociation energy  $D = 24$  kcal/mol, the frequency spectra of the local stretching modes  $q_1$  and

$q_2$  have largely delocalized across the entire frequency spectrum with broad peaks near  $\sim 400$   $\text{cm}^{-1}$  and  $\sim 900$   $\text{cm}^{-1}$ , while there are a couple of prominent, broadened peaks around  $500$   $\text{cm}^{-1}$  to  $600$   $\text{cm}^{-1}$  in  $q_3$ . These broadened peaks are reflected in the  $x$ -polarized infrared spectrum, while in the  $y$ -polarized infrared spectrum, we note broad peaks at  $\sim 400$   $\text{cm}^{-1}$  and  $\sim 900$   $\text{cm}^{-1}$ , just as in  $q_1$  and  $q_2$ . Finally, in Fig. 5(f), we reproduce Fig. 2 containing the frequency spectra for energy of 34 kcal/mol showing the emergence of resonance traps for long-lived trajectories with energies exceeding the dissociation energy.

### Appendix C: Estimating the Rabi splitting

We demonstrate how to estimate the Rabi splitting induced by the cavity mode in the infrared spectrum of the

vibrational modes in a manner similar to Refs. 19, 55, 56. As an example, we assume that the single cavity mode  $c$  is aligned along the in-plane axis through the center of the Bunker model to  $q_3/2$ , such that the only component of the permanent dipole moment  $\mu$  relevant to light-matter coupling is given by  $A \cos(q_3/2)(q_1 + q_2)$ , where the coefficient  $A$  is fitted with experimental or computational data describing the permanent dipole moment of ozone at vibrational equilibrium. With these simplifications, we can re-write  $H_F$  as

$$H_F = \frac{1}{2}\omega_c^2 q_c^2 + \frac{1}{2}p_c^2 + \frac{1}{2}\mu^2 \lambda_c^2 - \omega_c \mu \lambda_c q_c. \quad (\text{C1})$$

The first two terms correspond to the classical total energy of the cavity mode, the third term is the dipole self-energy term more relevant in the ultrastrong coupling limit, and the last term,  $H_{LM}$ , is the conventional light-matter interaction term on which we now focus our attention. To make further analytical progress, we assume that the molecule is close to its vibrational equilibrium state. By doing so, we can approximate the permanent dipole moment as  $\mu \approx \mu_0 + \frac{\partial \mu}{\partial q}|_{q_0}(q - q_0)$  where  $q$  is a generalized vibrational coordinate. Whether this assumption holds depends on the degree of vibrational excitation. For instance, this assumption encounters no issues with considering solely thermal population in the Bunker model, where the harmonic vibrational frequencies are several times higher than  $k_B T$ . However, in our numerical studies, the molecules are initialized with energies larger than the dissociation energy that is itself several times larger than the vibrational frequencies, so throughout the IVR process, the vibrational mode displacements from equilibrium can be large. Nonetheless, for the purpose of providing a simple, analytic form of the Rabi splitting that can be generalized to higher orders if necessary, we plug this term into  $H_{LM}$ :

$$H_{LM} = - \left[ \omega_c \mu_0 \lambda_c q_c + \frac{\partial \mu}{\partial q}|_{q_0} (q - q_0) \omega_c \lambda_c q_c \right]. \quad (\text{C2})$$

The latter term corresponds to the coupling between a vibrational transition and the cavity photon, and the Rabi splitting energy should correspond to the scaling factor of this term. We replace  $q_c$  and  $q$  with quantized field operators:

$$\frac{\partial \mu}{\partial q}|_{q_0} \omega_c q \lambda_c q_c = \frac{\partial \mu}{\partial q}|_{q_0} \omega_c \sqrt{\frac{\hbar}{2M\omega_v}} (\hat{b}^\dagger + \hat{b}) \lambda_c \sqrt{\frac{\hbar}{2\omega_c}} (\hat{a}_c^\dagger - \hat{a}_c), \quad (\text{C3})$$

where  $M$  is the effective mass of the vibration,  $\omega_v$  is the frequency of the vibration, and  $\hat{b}$  and  $\hat{a}_c$  are the annihilation operators of the vibrational and cavity modes, respectively.

We collect all the non-operator terms, multiply by a factor of two, and call this term the estimated Rabi splitting energy:

$$\hbar \Omega_R^{\text{est}} = \frac{\partial \mu}{\partial q}|_{q_0} \hbar \lambda_c \sqrt{\frac{\omega_c}{M\omega_v}}. \quad (\text{C4})$$

In our numerical studies, we have found that the cavity mode influences the unimolecular dissociation rate most strongly when the cavity is resonant with a junction dominated by the local mode vibration, such as  $q_3$  when the cavity is  $x$ -polarized, especially for vanishing local vibrational mode-mode momentum coupling  $\epsilon$ . Therefore, for the cavity field along the  $x$ -direction we approximate  $\frac{\partial \mu}{\partial q}|_{q_0}$  as

$$\frac{\partial \mu}{\partial q}|_{q_0} \approx \frac{\partial \mu}{\partial q_3}|_{q_3^0} = -A \sin(q_3^0/2)(q_1^0 + q_2^0)/2. \quad (\text{C5})$$

We estimate the Rabi splitting for typical parameters used in our numerical studies in atomic units, where  $\hbar = 1$ . For instance, for  $A = 0.395$  so that the permanent dipole moment at equilibrium  $\mu_0$  is 1,  $q_1^0 = q_2^0 = 2.416$ ,  $q_3^0 = 2.039$ ,  $M_{q_3} = 1/G_{33}^{(0)} = (2.88 \cdot 10^{-5})^{-1}$ ,  $\omega_3 = \omega_c = 2.88 \cdot 10^{-3}$ , and  $\lambda_c = 0.01$ , we estimate a Rabi splitting  $\hbar \Omega_R^{\text{est}} = 4.364 \cdot 10^{-5}$  in atomic units or  $9.577 \text{ cm}^{-1}$ . Because  $\hbar \Omega_R^{\text{est}}/\hbar \omega_3 \ll 0.1$ , the studied conditions are well below the ultra-strong coupling regime. This estimate indeed matches the splittings observed in Fourier transforms of the vibrational coordinates of the coupled molecule-cavity system under the conditions described, as in Fig. 6, where the molecule is initialized with energy  $\ll \hbar \omega_i$  to prevent the appearance of overtones and combination spectra. We propagate the same initial condition for all  $\lambda_c$ :  $\{p_1, p_2, p_3, q_1, q_2, q_3, p_c, q_c\} = \{5, 5, -5, 2.8, 2.8, 2, 0.01, 0.01, 0, 0\}$  in atomic units.

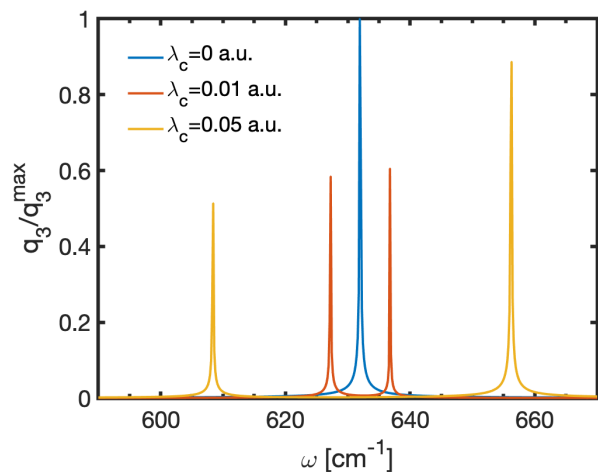


**FIG. 6.** Rabi splitting of the local bending mode  $q_3$  for the molecular model  $\epsilon = 0$  and low energy such that the vibrational coordinates are close to equilibrium. The molecule is placed inside a cavity with frequency  $\omega_c = \omega_3$  for varying cavity strength  $\lambda_c$ . The estimated Rabi splitting  $\hbar \Omega_R^{\text{est}} \sim 10 \text{ cm}^{-1}$  for  $\lambda_c = 0.01$ , closely matching the actual Rabi splitting observed.

- 
- [1] H. Frei, L. Fredin, and G. C. Pimentel, Vibrational excitation of ozone and molecular fluorine reactions in cryogenic matrices, *Journal of Chemical Physics* **74**, 397 (1980).
- [2] H. Frei and G. C. Pimentel, Selective vibrational excitation of the ethylene-fluorine reaction in a nitrogen matrix. I, *Journal of Chemical Physics* **7**, 3698 (1983).
- [3] H. Frei, Selective vibrational excitation of the ethylene-fluorine reaction in a nitrogen matrix. II, *Journal of Chemical Physics* **79**, 748 (1983).
- [4] P. H. Bucksbaum, A. Zavriyev, H. G. Muller, and D. W. Schumacher, Softening of the  $H_2^+$  Molecular Bond in Intense Laser Fields, *Physical Review Letters* **64**, 1883 (1990).
- [5] P. Brumer and M. Shapiro, Control of unimolecular reactions using coherent light, *Chemical physics letters* **126**, 541 (1986).
- [6] W. S. Warren, H. Rabitz, and M. Dahleh, Coherent Control of Quantum Dynamics: The Dream Is Alive, *Science* **259**, 1581 (1993).
- [7] T. Uzer and W. H. Miller, Theories of intramolecular vibrational energy transfer, *Physics Reports* **199**, 73 (1991).
- [8] A. Thomas, L. Lethuillier-Karl, K. Nagarajan, R. M. Vergauwe, J. George, T. Chervy, A. Shalabney, E. Devaux, C. Genet, J. Moran, and T. W. Ebbesen, Tilting a ground-state reactivity landscape by vibrational strong coupling, *Science* **363**, 615 (2019).
- [9] A. Thomas, A. Jayachandran, L. Lethuillier-Karl, R. M. Vergauwe, K. Nagarajan, E. Devaux, C. Genet, J. Moran, and T. W. Ebbesen, Ground state chemistry under vibrational strong coupling: Dependence of thermodynamic parameters on the Rabi splitting energy, *Nanophotonics* **9**, 249 (2020).
- [10] K. Hirai, R. Takeda, J. A. Hutchison, and H. Uji-i, Modulation of Prins Cyclization by Vibrational Strong Coupling, *Angewandte Chemie - International Edition* **59**, 5332 (2020).
- [11] Y. Pang, A. Thomas, K. Nagarajan, R. M. A. Vergauwe, K. Joseph, B. Patrahaui, K. Wang, C. Genet, and T. W. Ebbesen, On the Role of Symmetry in Vibrational Strong Coupling: The Case of Charge-Transfer Complexation, *Angewandte Chemie* **132**, 10522 (2020).
- [12] A. Sau, K. Nagarajan, B. Patrahaui, L. Lethuillier-Karl, R. M. A. Vergauwe, A. Thomas, J. Moran, C. Genet, and T. W. Ebbesen, Modifying Woodward–Hoffmann Stereoselectivity Under Vibrational Strong Coupling, *Angewandte Chemie* **133**, 5776 (2021).
- [13] D. S. Wang and S. F. Yelin, A roadmap toward the theory of vibrational polariton chemistry, *arXiv:2107.09026*, 1 (2021).
- [14] J. Feist, J. Galego, and F. J. Garcia-Vidal, Polaritonic Chemistry with Organic Molecules, *ACS Photonics* **5**, 205 (2018).
- [15] J. Flick, N. Rivera, and P. Narang, Strong light-matter coupling in quantum chemistry and quantum photonics, *Nanophotonics* **7**, 1479 (2018).
- [16] R. F. Ribeiro, L. A. Martínez-Martínez, M. Du, J. Campos-Gonzalez-Angulo, and J. Yuen-Zhou, Polariton chemistry: controlling molecular dynamics with optical cavities, *Chemical Science* **9**, 6325 (2018).
- [17] F. Herrera and J. Owrutsky, Molecular polaritons for controlling chemistry with quantum optics, *Journal of Chemical Physics* **152**, 100902 (2020).
- [18] F. J. Garcia-vidal, C. Ciuti, and T. W. Ebbesen, Manipulating matter by strong coupling to vacuum fields, *Science* **178**, 1 (2021).
- [19] J. Galego, C. Climent, F. J. Garcia-Vidal, and J. Feist, Cavity Casimir-Polder Forces and Their Effects in Ground-State Chemical Reactivity, *Physical Review X* **9**, 021057 (2019).
- [20] J. A. Campos-Gonzalez-Angulo, R. F. Ribeiro, and J. Yuen-Zhou, Resonant catalysis of thermally activated chemical reactions with vibrational polaritons, *Nature Communications* **10**, 1 (2019).
- [21] T. E. Li, A. Nitzan, and J. E. Subotnik, On the origin of ground-state vacuum-field catalysis: Equilibrium consideration, *Journal of Chemical Physics* **152**, 234107 (2020).
- [22] X. Li, A. Mandal, and P. Huo, Cavity frequency-dependent theory for vibrational polariton chemistry, *Nature Communications* **12**, 1 (2021).
- [23] X. Li, A. Mandal, and P. Huo, Mode-selective chemistry through polaritonic vibrational strong coupling (2021).
- [24] C. Schäfer, J. Flick, E. Ronca, P. Narang, and A. Rubio, Shining Light on the Microscopic Resonant Mechanism Responsible for Cavity-Mediated Chemical Reactivity, *arXiv:2104.12429* (2021).
- [25] M. Du and J. Yuen-Zhou, Can Dark States Explain Vibropolaritonic Chemistry?, *arXiv:2104.07214* (2021).
- [26] A. Mandal, X. Li, and P. Huo, Theory of Vibrational Polariton Chemistry in the Collective Coupling Regime, *arXiv:2107.04156*, 1 (2021).
- [27] K. Head-Marsden, J. Flick, C. J. Ciccarino, and P. Narang, Quantum Information and Algorithms for Correlated Quantum Matter, *Chemical Reviews* **121**, 3061 (2021).
- [28] T. E. Li, J. E. Subotnik, and A. Nitzan, Cavity molecular dynamics simulations of liquid water under vibrational ultrastrong coupling, *Proceedings of the National Academy of Sciences of the United States of America* **117**, 18324 (2020).
- [29] T. E. Li, A. Nitzan, and J. E. Subotnik, Energy-efficient pathway for selectively exciting solute molecules to high vibrational states via solvent vibration-polariton pumping, *arXiv:2104.15121*, 1 (2021).
- [30] T. E. Li, A. Nitzan, and J. E. Subotnik, Cavity molecular dynamics simulations of vibrational polariton-enhanced molecular nonlinear absorption, *Journal of Chemical Physics* **154**, 094124 (2021).
- [31] T. E. Li, A. Nitzan, and J. E. Subotnik, Collective Vibrational Strong Coupling Effects on Molecular Vibrational Relaxation and Energy Transfer: Numerical Insights via Cavity Molecular Dynamics Simulations, *Angewandte Chemie* **133**, 15661 (2021).
- [32] J. Flick, M. Ruggenthaler, H. Appel, and A. Rubio, Atoms and molecules in cavities, from weak to strong coupling in quantum-electrodynamics (QED) chemistry, *Proc. Natl. Acad. Sci. U.S.A.* **114**, 3026 (2017).
- [33] J. Flick and P. Narang, Cavity-correlated electronuclear dynamics from first principles, *Phys. Rev. Lett.* **121**, 113002 (2018).
- [34] A. Thomas, J. George, A. Shalabney, M. Dryzhakov,

- S. J. Varma, J. Moran, T. Chervy, X. Zhong, E. Devaux, C. Genet, J. A. Hutchison, and T. W. Ebbesen, Ground-State Chemical Reactivity under Vibrational Coupling to the Vacuum Electromagnetic Field, *Angewandte Chemie - International Edition* **55**, 11462 (2016).
- [35] S. Karmakar, P. K. Yadav, and S. Keshavamurthy, Stable chaos and delayed onset of statisticality in unimolecular dissociation reactions, *Communications Chemistry* **3**, 1 (2020).
- [36] D. L. Bunker, Monte Carlo Calculation of Triatomic Dissociation Rates. I. N<sub>2</sub>O and O<sub>3</sub>, *The Journal of Chemical Physics* **37**, 393 (1962).
- [37] D. L. Bunker, Monte Carlo Calculations. IV. Further Studies of Unimolecular Dissociation, *The Journal of Chemical Physics* **40**, 1946 (1964).
- [38] D. W. Oxtoby and S. A. Rice, Nonlinear resonance and stochasticity in intramolecular energy exchange, *The Journal of Chemical Physics* **65**, 1676 (1976).
- [39] C. Froeschle, M. Guzzo, and E. Lega, Graphical evolution of the Arnold web: From order to chaos, *Science* **289**, 2108 (2000).
- [40] P. Manikandan and S. Keshavamurthy, Dynamical traps lead to the slowing down of intramolecular vibrational energy flow, *Proceedings of the National Academy of Sciences of the United States of America* **111**, 14354 (2014).
- [41] P. C. Cross and J. H. Van Vleck, Molecular vibrations of three particle systems with special applications to the ethyl halides and ethyl alcohol, *The Journal of Chemical Physics* **1**, 350 (1933).
- [42] T. Uzer, G. A. Natanson, and J. T. Hynes, Coriolis-induced intramolecular vibrational energy flow between anharmonic normal modes, *Chemical Physics Letters* **122**, 12 (1985).
- [43] J. R. Dormand and P. J. Prince, High order embedded Runge-Kutta formulae, *Journal of Computational and Applied Mathematics* **7**, 67 (1981).
- [44] S. M. Adler-Golden, S. R. Langhoff, C. W. Bauschlicher, and G. D. Carney, Theoretical calculation of ozone vibrational infrared intensities, *The Journal of Chemical Physics* **83**, 255 (1985).
- [45] S. L. Shostak, W. L. Ebenstein, and J. S. Muentzer, The dipole moment of water. I. Dipole moments and hyperfine properties of H<sub>2</sub>O and HDO in the ground and excited vibrational states, *The Journal of Chemical Physics* **94**, 5875 (1991).
- [46] J. Lather, P. Bhatt, A. Thomas, T. W. Ebbesen, and J. George, Cavity Catalysis by Cooperative Vibrational Strong Coupling of Reactant and Solvent Molecules, *Angewandte Chemie - International Edition* **58**, 10635 (2019).
- [47] B. Xiang, R. F. Ribeiro, M. Du, L. Chen, Z. Yang, J. Wang, J. Yuen-Zhou, and W. Xiong, Intermolecular vibrational energy transfer enabled by microcavity strong light-matter coupling, *Science* **368**, 665 (2020).
- [48] S. Schütz, J. Schachenmayer, D. Hagenmüller, G. K. Brennen, T. Volz, V. Sandoghdar, T. W. Ebbesen, C. Genes, and G. Pupillo, Ensemble-Induced Strong Light-Matter Coupling of a Single Quantum Emitter, *Physical Review Letters* **124**, 113602 (2020).
- [49] D. Sidler, C. Schäfer, M. Ruggenthaler, and A. Rubio, Polaritonic Chemistry: Collective Strong Coupling Implies Strong Local Modification of Chemical Properties, *Journal of Physical Chemistry Letters* **12**, 508 (2021).
- [50] H. L. Luk, J. Feist, J. J. Toppari, and G. Groenhof, Multiscale Molecular Dynamics Simulations of Polaritonic Chemistry, *Journal of Chemical Theory and Computation* **13**, 4324 (2017).
- [51] G. Groenhof, C. Climent, J. Feist, D. Morozov, and J. J. Toppari, Tracking Polariton Relaxation with Multiscale Molecular Dynamics Simulations, *Journal of Physical Chemistry Letters* **10**, 5476 (2019).
- [52] I. V. Tokatly, Time-dependent density functional theory for many-electron systems interacting with cavity photons, *Phys. Rev. Lett.* **110**, 233001 (2013).
- [53] M. Ruggenthaler, J. Flick, C. Pellegrini, H. Appel, I. V. Tokatly, and A. Rubio, Quantum-electrodynamical density-functional theory: Bridging quantum optics and electronic-structure theory, *Phys. Rev. A* **90**, 012508 (2014).
- [54] D. S. Wang, T. Neuman, J. Flick, and P. Narang, Light-matter interaction of a molecule in a dissipative cavity from first principles, *Journal of Chemical Physics* **154**, 104109 (2021).
- [55] A. Shalabney, J. George, J. Hutchison, G. Pupillo, C. Genet, and T. W. Ebbesen, Coherent coupling of molecular resonators with a microcavity mode, *Nature Communications* **6**, 1 (2015).
- [56] X. Li, A. Mandal, and P. Huo, Cavity frequency-dependent theory for vibrational polariton chemistry, *Nature Communications* **12**, 1 (2021).